Calcium-dependent regulation of auxin transport in plant development

Wei, X.

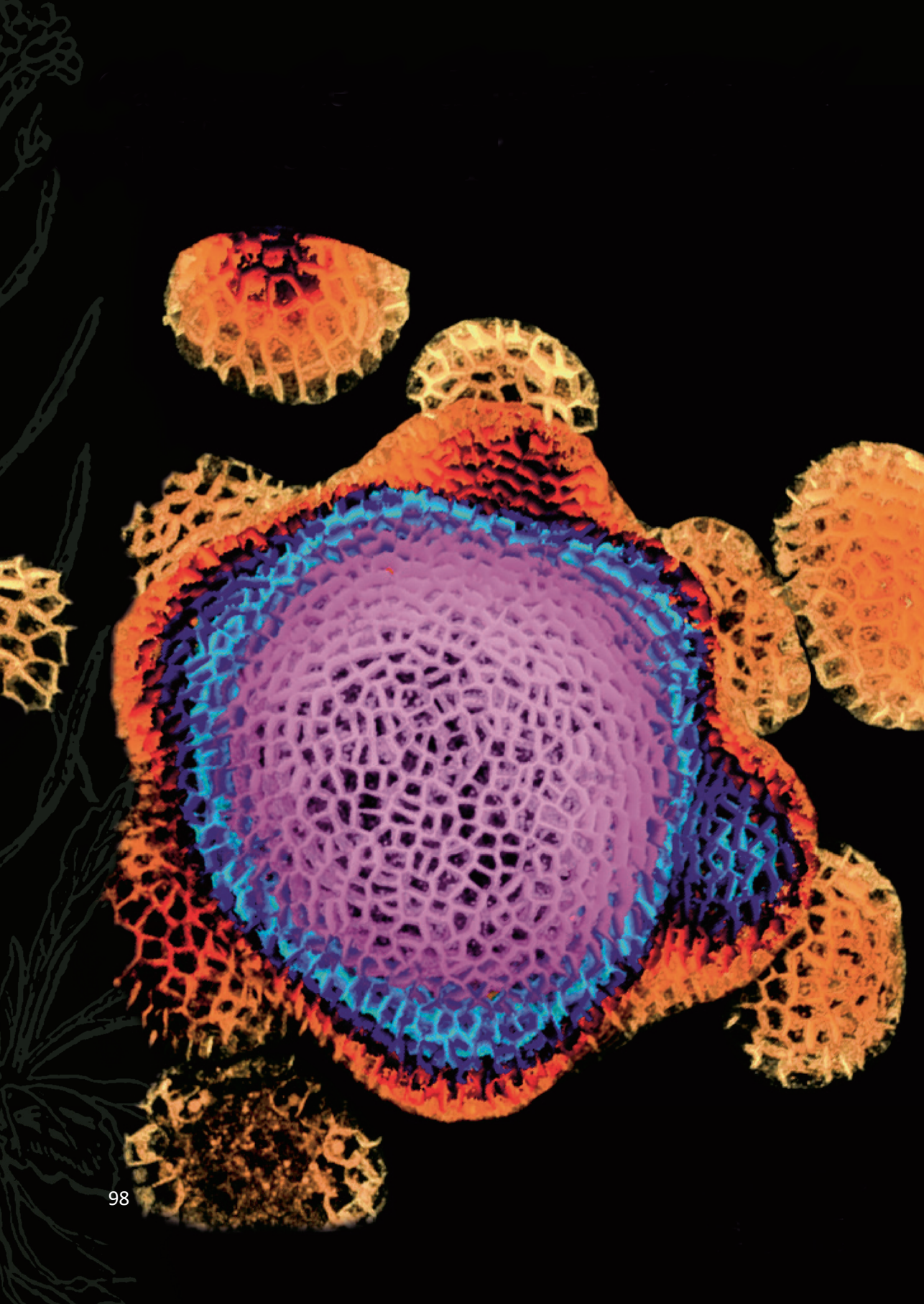

Chapter 3

PINOID plasma membrane association and CALMODULIN-LIKE 12/TOUCH 3 binding converge on an amphipathic alpha-helix in the kinase insertion domain

Xiaoyu Wei[1,4], Yuanwei Fan[2,4], Eike Rademacher[3,4] and Remko Offringa[1]*

[1] Plant Developmental Genetics, Institute of Biology Leiden, Leiden University, Sylviusweg 72, 2333 BE, Leiden, Netherlands

[2] Department of Biology and Center for Engineering Mechanobiology, Washington University in St. Louis, St. Louis, MO 63130, USA

[3] Rijk Zwaan, 2678 KX De Lier, The Netherlands

[4] These authors contributed equally to this manuscript

*Author for correspondence: r.offringa@biology.leidenuniv.nl

The results in this Chapter are included in the following publication: **Wei, X.Y.,** Fan, Y.W.,.….Offringa, R*. Calcium-regulated PINOID kinase activity is required for a robust spiral phyllotaxis in the Arabidopsis inflorescence (In preparation).

Abstract

The protein kinase PINOID (PID) is a plasma membrane (PM) associated AGC3 protein kinase that regulates auxin transport polarity by phosphorylating PIN auxin efflux carriers. Previous research and our results in Chapter 2 showed that a confined clade comprising seven CaMs and four closely-related calmodulin-like proteins (CMLs), including CALMODULIN-LIKE 12/TOUCH 3 (CML12/TCH3), interact with PID, and sequester PID from the PM to the cytosol. These PID interacting CaM/CMLs were found to be co-expressed with PID in many tissues, and the single loss-of-function mutants of the genes encoding PID interacting CaM/CMLs did not show a clear phenotype, suggesting that there is functional redundancy. In order to identify the biological function of the CaM/CML-PID interaction, we mapped the CaM/CMLs binding domain in PID. First, we confirmed that PID associates to the PM by the insertion domain (ID) in the catalytic kinase core. Subsequent fine mapping of the CaM/CML binding domain in PID showed that both CaM/CML binding and PM association converge at an amphipathic alpha helix in the PID ID. Disruption of this amphipathic alpha helix by substitution of several positively charged arginines by alanines (RtoA) interfered with both CaM/CML binding and PM association. Surprisingly, the PID(RtoA) versions showed the same overexpression phenotypes as wild-type PID and complemented the pin-like inflorescence phenotype of the *pid* mutant, when expressed under the *PID* promoter. Our results indicate that PM association is not essential for PID function and that the 'untouchable' PID(RtoA) versions are useful tools to study the role of the PID-CaM/CML interaction in plant development.

Keywords: PINOID (PID), AGC protein serine/threonine kinase, Calmodulin (CaM), Calmodulin-like (CML), Plasma membrane association, Amphipathic alpha helix, Arabidopsis

Introduction

The plant hormone auxin is a well-established inducer of Ca^{2+} signalling (Hasenstein and Evans, 1986; Felle, 1988; Gerring et al., 1990; Irving et al., 1992; Shishova and Lindberg, 1999; Monshausen et al., 2011). In fact, several reports indicate the involvement of Ca^{2+} signalling in the regulation of auxin transport during gravitropism (Dela Fuente and Leopold, 1973; Lee et al., 1984; Plieth and Trewavas, 2002; Toyota et al., 2008) and phototropism (Baum et al., 1999; Harada et al., 2003; Harada and Shimazaki, 2007; Zhao et al., 2013), and its requirement for the inhibitory effect of auxin on root and root hair growth via the nonselective cation channel CYCLIC NUCLEOTIDE-GATED CHANNEL 14 (CNGC14) (Shih et al., 2015; Dindas et al., 2018). Surprisingly, despite all these findings, molecular details about the role of Ca^{2+} signalling downstream of auxin and its cellular targets have remained elusive for a long time.

Previously, we identified the calmodulin-like protein CALMODULIN-LIKE 12/TOUCH 3 (CML12/TCH3) as interacting partner of the protein kinase PINOID (PID) (Benjamins et al., 2003). As PID is known to regulate polar auxin transport (PAT) by phosphorylating PIN proteins (Friml et al., 2004; Michniewicz et al., 2007; Huang et al., 2010), our findings provided one of the first molecular links between auxin and Ca^{2+} signalling. Calmodulins (CaMs) and calmodulin-like proteins (CMLs) are well-defined calcium sensors and central to the activation of calcium signalling pathways (Yang and Tsai, 2022). The crystal structure of CaM has revealed two globular domains, each containing two EF-hand Ca^{2+}-binding sites, connected by a linker (Babu et al., 1985; Chattopadhyaya et al., 1992; Kretsinger et al., 1986; Babu et al.,1988; Tidow and Nissen, 2013). CMLs have a similar structure and only vary in the number of EF hands (McCormack and Braam, 2003). CaM/CMLs respond rapidly to oscillations in the cytosolic Ca^{2+} levels ($[Ca^{2+}]_{cyt}$). Binding of Ca^{2+} to the EF-hands triggers a more open conformation, exposing the methionine-rich hydrophobic pockets in each globular

domain (Crivici and Ikura, 1995; Zhang et al., 1995). These stretches of methionines have high polarizability and flexibility, and their increased accessibility allows CaM/CMLs to undergo extensive protein-protein interactions (Gellman, 1991; Zhang et al., 1994; Zhang and Vogel, 1994; Yamniuk and Vogel, 2004).

PID belongs to the AGC3 subclade of plant-specific AGCVIII protein serine-threonine kinase family (Galvan-Ampudia and Offringa, 2007). AGCVIII kinases distinguish themselves from other (non-plant) AGC kinases by an insertion domain (ID) between catalytic subdomain VII and VIII, ranging in size from 36 to 90 amino acid residues (Bögre et al., 2003; Galván-Ampudia and Offringa, 2007; Rademacher and Offringa, 2012). Previous data already indicated that the insertion domain (ID) is responsible for PID plasma membrane (PM) association (Zegzouti et al., 2006). The results in Chapter 2 showed that PID not only interacts with CML12/TCH3 but also with all seven CaMs and three other CMLs (CML8, CML10, CML11), all belonging to a confined clade of closely related CaM/CMLs in Arabidopsis. Through this interaction PID is sequestered from the PM to the cytosol, suggesting that these CaM/CMLs bind to the insertion domain and thereby disrupt its PM association. In addition, we have shown that these PID interacting CaM/CMLs are co-expressed with PID in many tissues, such as the shoot apical meristem, vascular tissues, young developing leaves and flowers, enabling a functional interaction between PID and these CaM/CMLs in these tissues. Unfortunately, the single loss-of-function mutants for *CML12/TCH3* or for the other genes encoding PID interacting CaM/CMLs did not show a clear phenotype, and together with their overlapping expression pattern this suggests that they act redundantly (Chapter 2). With the current CRISPR-Cas tool-box, it would be easy to generate multiple CaM/CML mutants to investigate the role of the CaM/CML-PID interaction in plant growth and development. However, CaM/CMLs generally interact with and regulate multiple proteins and are thus involved in many calcium-dependent signalling pathways (Perochon et al., 2011).

Therefore, a knock-out of all the genes encoding PID-interacting CaM/CMLs is very likely to lead to severe defects. In fact, knocking out the single *CaM* gene in *Saccharomyces cerevisiae* (Davis et al., 1986), *Schizosaccharomyces pombe* (Takeda and Yamamoto, 1987), *Aspergillus nidulans* (Lu et al., 1992) and *Drosophila melanogaster* (Heiman et al., 1996) appeared to be lethal. Therefore, we decided to map the CaM/CMLs-binding domain in PID in order to identify the key amino acids responsible for CaM/CMLs-binding, with the final aim to generate an 'untouchable' but still fully functional version of PID. Complementation of the *pid* loss-of-function mutant should then reveal the role of the calcium-dependent CaM/CML binding to PID.

In this Chapter, we fine mapped the CaM/CML binding domain in PID through amino acid deletions and substitutions. Subsequent protein domain modelling identified an amphipathic alpha helix in the ID of PID that mediates both PM association and the interaction with the CaM/CMLs. Substitution of the positively charged arginines in this alpha helix resulted in the desired 'untouchable' PID, which will enable us to finally unravel the role of the calcium-dependent PID-CaM/CML interaction in plant development (see Chapter 4).

Results

PID PM association and CML12/TCH3 interaction are both mediated by the ID in the catalytic kinase core

To confirm the initial observations that PM association of PID is mediated by the ID (Zegzouti et al., 2006), we fused the ID (AA 227 to 280) to YFP. Expression of this fusion under the *35S* promotor in Arabidopsis protoplasts showed similar PM association as the PID-YFP fusion (Figure 1A, B), thereby confirming that the ID is responsible for PM association. Moreover, expression of a PID-YFP fusion lacking the ID (PID(-ID)-YFP) resulted in cytosolic localisation, whereas a fusion with the ID reintroduced (PID(+ID)-YFP) showed again the same PM association

as the PID-YFP and ID-YFP fusions (Figure 1A, B). To verify our hypothesis that CaM/CMLs bind to the ID of PID, *in vitro* pull-down assays were performed with GST-tagged PID, PID(-ID), PID(+ID) and ID alone bound to glutathione beads as bait and His-tagged CML12/TCH3 as prey. These experiments showed that CML12/TCH3 can be pulled down by GST-PID when the ID is present and even more efficient by the GST-ID fusion, but not by the GST-PID version lacking the ID. (Figure 1C). These results indicated that both the PM association and the CaM/CML binding domains are located in the ID of PID.

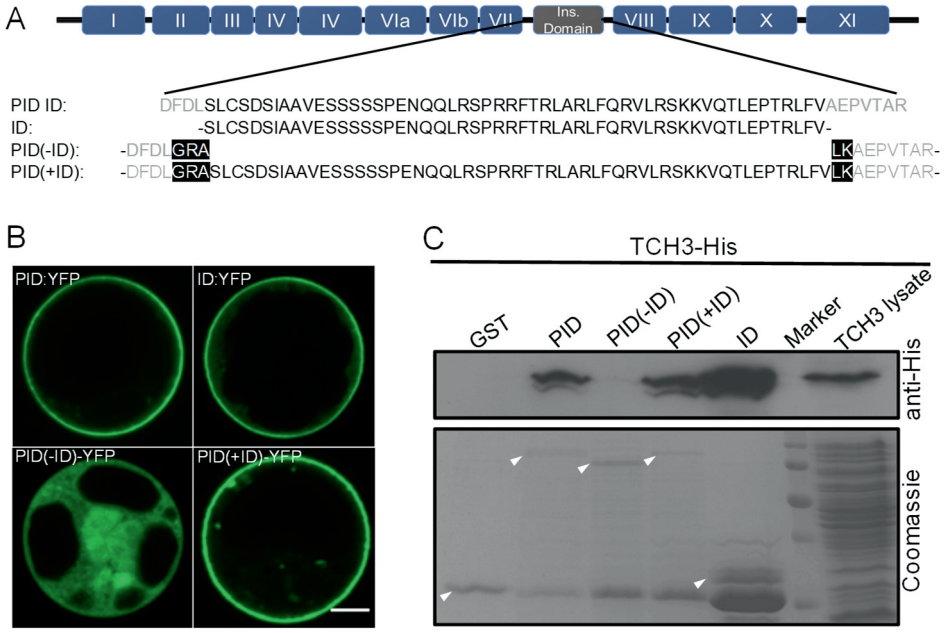

Figure 1. The ID in the catalytic core of the PID kinase mediates both PM association and CaM/CML binding. (A) Schematic structure of the PID kinase with the 12 conserved domains of the catalytic core and the ID indicated (above) and amino acid sequence of the PID ID and PID mutant versions. **(B)**. Arabidopsis protoplasts transfected with *p35S:PID-YFP, p35S:ID-YFP, p35S:PID(-ID)-YFP, p35S:PID(+ID)-YFP*. The scale bar indicates 10 µm. **(C)** *In vitro* pull-down using GST, GST-PID (PID), GST-PID(-ID) (PID(-ID)), GST-PID with the ID placed back (PID(+ID)) or GST-ID (ID) bound to glutathione beads as bait and His-tagged TCH3 as prey. Upper image: pulled down TCH3-His detected by hybridizing the Western blot with anti-His antibodies. Lower image: Coomassie stained gel showing the loading of glutathione beads with GST-tagged proteins. White arrowheads indicate the positions of the respective GST-tagged proteins.

Central segment in the PID ID is sufficient for PM association and CML12/TCH3 binding

Previous studies on CaM/CML binding domains have indicated that CaM/CMLs interact with two types of motifs: the amphipathic alpha helix and the IQ or IQ-like motif (O'Neil and DeGrado, 1990; Clore et al., 1993; Rhoads and Friedberg, 1997; Bähler and Rhoads, 2002; Yamniuk and Vogel, 2004; Ranty et al., 2006; Andrews et al., 2020). To our surprise, analysis of the PID ID detected an alpha helix (amino acid residues 249 to 266) that partially overlapped with an IQ-like motif (amino acid residues 261 to 273) (Figure 2A). Visualization of the predicted alpha helix in the central segment using helical wheel projection software indicated the presence of a perfect amphipathic alpha helix comprising amino acid residues 249 to 266 (RSPRRFTRLARLFQRVLR), with the key features of seven positively charged amino acids on one side, and six hydrophobic amino acids on the other side (Figure 2B, C).

A segment containing this amphipathic alpha helix and IQ-like motif (amino acid residues 244 to 275) was fused to GST ($ID_{244-275}$) for *in vitro* pull-down and to YFP ($ID_{244-275}$-YFP) for expression in protoplasts under the *35S* promoter. The pull-down result indicated that the short segment is sufficient for interacting with CML12/TCH3 (Figure 2D), and expression of the $ID_{244-275}$-YFP fusion in Arabidopsis protoplasts showed that it was sufficient for PM association (Figure 2E). In Chapter 2 we showed that PID was sequestered from the PM to the cytosol when co-expressed in Arabidopsis protoplasts with CML12/TCH3 in an auxin-dependent manner. Co-expression of either the full length ID-YFP or the shorter $ID_{244-275}$-YFP fusion with CML12/TCH3 in Arabidopsis protoplast showed that, like the full-length ID, also the shorter $ID_{244-275}$ fragment could be sequestered from the PM to the cytosol when auxin was added to the protoplasts (Figure 2F). Together these data suggest that the $ID_{244-275}$ segment comprising the amphipathic alpha helix and IQ-like motif mediates both PM association and CaM/CML binding.

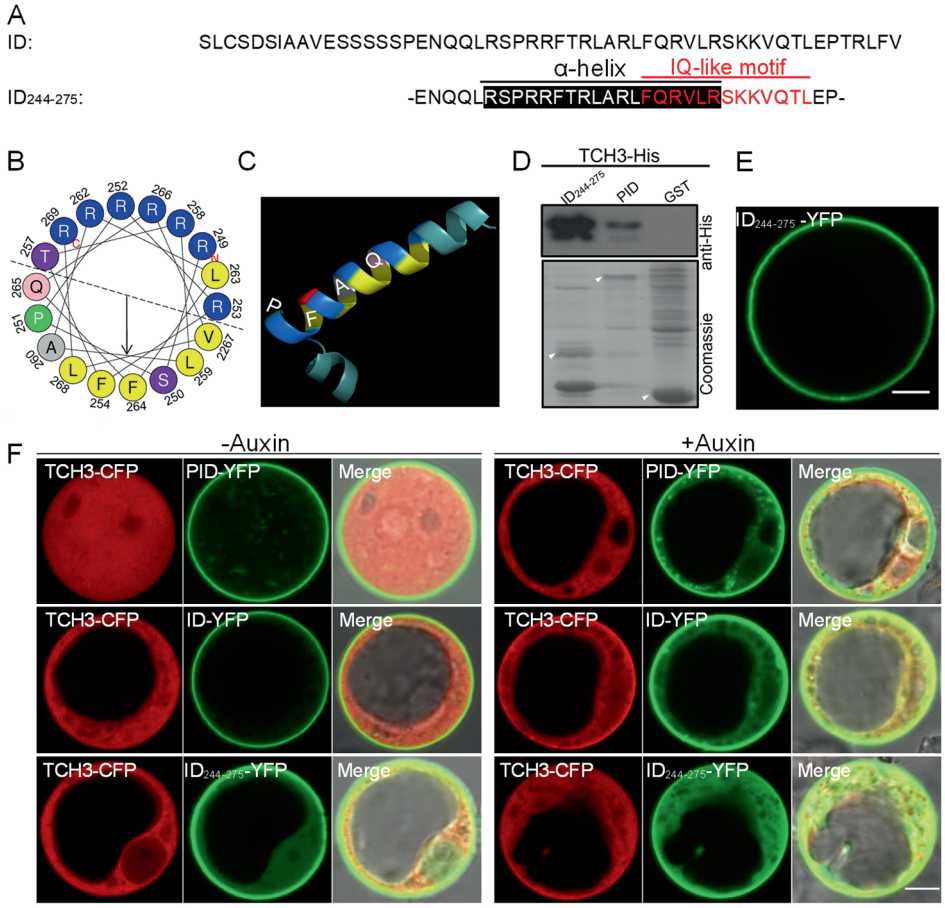

Figure 2. Central segment in the PID ID containing an alpha-helix and an IQ-like domain is sufficient for PM association and CaM/CML binding. (A) Amino acid sequence of the PID ID and the central segment (AA 244-275) containing the alpha-helix (white letters on a black background) and IQ-like motif (red letters). **(B, C)** Alpha helix projection **(B)** and protein structure prediction **(C)** indicate that amino acid residues 249 to 266 in the PID ID contain a perfect amphipathic alpha helix. Positively charged residues are in blue, hydrophobic residues are in yellow or grey, serine (S) and threonine (T) are in purple, green for proline (P) and pink for glutamic acid (Q). The numbers in **(B)** indicate the order of the amino acids in the sequence. Color coding in **(C)**: blue indicates basic/hydrophillic residues, yellow indicates hydrophobic residues, red indicates the threonine residue. **(D).** *In vitro* pull-down using GST, GST-PID (PID), or GST-ID (ID) bound to glutathione beads as bait and His-tagged TCH3 as prey. Pulled down TCH3-His was detected by Western blot hybridized with anti-His antibodies. White arrowheads indicate the positions of the respective GST-tagged proteins. **(E)** Arabidopsis protoplast expressing $ID_{244-275}$-YFP. **(F)** Auxin-starved (left panel) and auxin-supplemented (right panel) Arabidopsis protoplasts co-transfected with *p35S:PID-YFP, p35S:ID-YFP, p35S:ID -YFP, p35S: $ID_{244-275}$-YFP* and *p35S:TCH3-CFP*. The scale bar in (**E**) and (**F**) indicates 10 µm.

Apart from binding CaM/CMLs, amphipathic alpha helices are also known for mediating PM association of proteins (Zhukovsky et al., 2019), whereas IQ-like motifs are specific for CaM/CML binding. The presence of an overlapping amphipathic alpha helix and an IQ-like motif in the PID ID suggested that the first might be involved in PM association, whereas the latter mediated the CaM/CML binding. To test this, we generated PID mutant versions with amino acid substitutions at the C-terminus of the IQ-like motif that did not disrupt the amphipathic alpha helix (Figure S1A). The substitutions were selected based on previous findings that CaM/CMLs bind their target proteins either through hydrophobic interactions (e.g. V, L) or through electrostatic interactions (e.g. K) (O'Neil and DeGrado, 1990; Crivici and Ikura, 1995; Bähler and Rhoads, 2002; Rhoads and Friedberg, 1997; Poovaiah et al., 2013; Andrews et al., 2020). In the mutant PID versions PID K268A, PID K269A and PID K268269A the positively charged lysines (K) were therefore substituted with neutral alanines (A), and in mutant PID versions PID V270D, PID V270D/L273E, the hydrophobic amino acids valine (V) and leucine (L) were substituted with the hydrophilic/negatively charged amino acids aspartic acid (D) or glutamic acid (E), respectively.

In vitro pull-downs showed that all these mutants (PID(K268A), PID(K269A), PID (K268,269A), PID(V270D), PID(V270D/L273E) could still interact with CML12/TCH3 (Figure S1C). Expression of the YFP fusions of these mutant PID versions in Arabidopsis protoplasts showed mainly PM localization (Figure S1B). These results suggest that the IQ-like motif may not be involved in CML12/TCH3 binding nor in PM association.

To confirm these results and further map the CaM/CML binding domain, we replaced the PID ID with three smaller segments: PID(+$ID_{227-253}$), PID(+$ID_{240-266}$) or PID(+$ID_{254-280}$) (Figure 3A). *In vitro* pull-downs and Arabidopsis protoplast transfection assays showed that only the PID(+$ID_{240-266}$) version (including amphipathic alpha helix, but excluding the C-terminal half of the IQ-like motif) was able to interact with CML12/TCH3 and show PM association (Figure 3B, C).

Taken together, these results indicate that the central segment of the PID ID harbouring an amphipathic alpha helix is sufficient and necessary for both PM association and CML12/TCH3 binding.

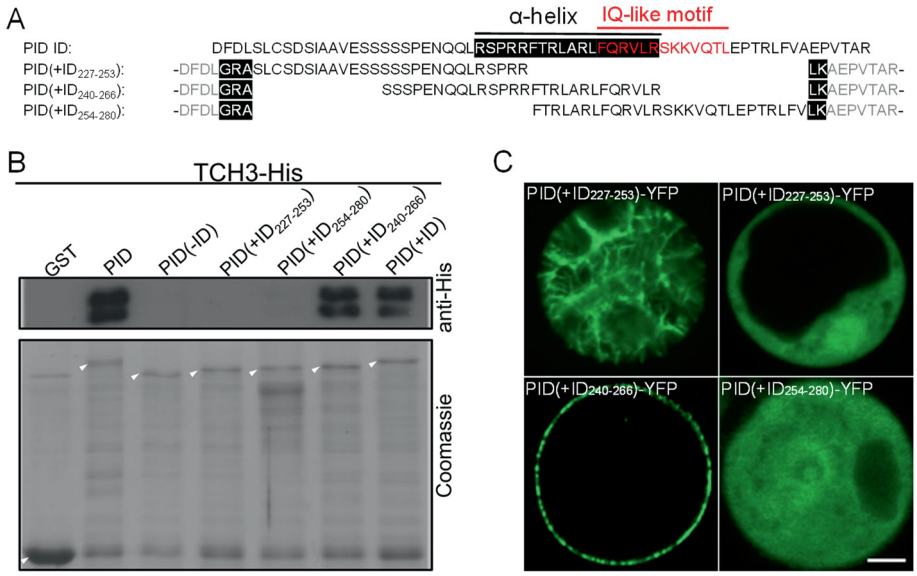

Figure 3. Central segment of the PID ID containing the amphipathic alpha-helix is sufficient and necessary for both PM association and CaM/CML binding. (A) Amino acid sequence of PID ID and different PID mutant versions. **(B).** *In vitro* pull-down using GST, GST-PID (PID), GST-PID without ID (PID-ID), GST-PID minus ID with three smaller segments replaced back (PID(+ID$_{227-253}$), PID(+ID$_{240-266}$), and PID(+ID$_{254-280}$)) bound to glutathione beads as bait and His-tagged TCH3 as prey. Pulled down TCH3-His was detected by Western blot hybridized with anti-His antibodies. White arrowheads indicate the positions of the respective GST-tagged proteins. **(C)** Arabidopsis protoplasts transfected with *p35S: PID(+ID$_{227-253}$)-YFP*, *p35S: PID(+ID$_{240-266}$)-YFP*, *p35S: PID(+ID$_{254-280}$)-YFP*. The scale bar indicates 10 µm.

PM association and CML12/TCH3 binding converge at the amphipathic alpha helix in the PID ID

Alanine scanning has been widely employed as a method of exploration of protein-protein binding interfaces (Lefèvre et al., 1997). To further analyse the central segment in the PID ID and validate the importance of the predicted amphipathic alpha helix in CaM/CMLs binding and PM association, three successive stretches of seven amino acids in the central segment were substituted with alanines, resulting in respectively PID Ala1 (QLRSPRR), PID Ala2 (FTRLARL) and PID

Ala3 (FQRVLRS) (Figure 4A). The N-terminal part of the central fragment (SSSPENQ) was ignored, as it did not contain amino acids typical for CaM/CML binding or PM association. Interestingly, none of the three PID alanine mutant versions showed *in vitro* interaction with CML12/TCH3 (Figure 4C), nor did they associate with the PM (Figure 4B). These data confirmed that the complete predicted amphipathic alpha helix is crucial for CaM/CMLs binding and PM association.

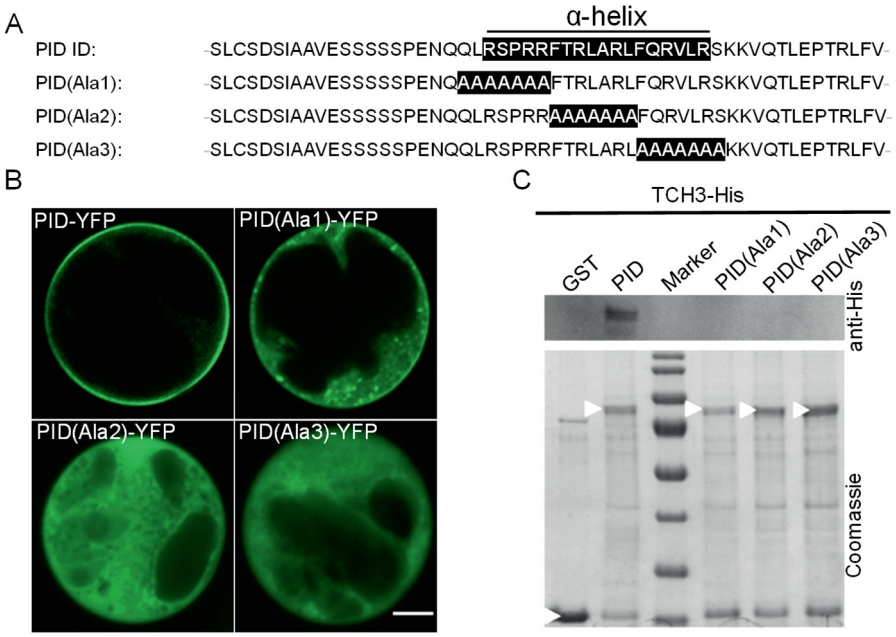

Figure 4. The complete amphipathic alpha-helix in the PID ID is required for PM association and CML12/TCH3 binding. (A). Amino acid sequence of the PID ID and the three PID Ala mutant versions. The amphipathic alpha helix and the alanine substitutions are indicated with white letters on a black background. **(B)** Arabidopsis protoplasts transfected with *p35S:PID Ala1-YFP, p35S:PID Ala2-YFP* and *p35S:PID Ala3-YFP*. The scale bar indicates 10 µm. **(C)** *In vitro* pull-down using GST, GST-PID (PID), GST-PID with alanine scanned ID (PID(Ala1), PID(Ala2), PID(Ala3) bound to glutathione beads as bait and His-tagged TCH3 as prey. Pulled down TCH3-His was detected by Western blot hybridized with anti-His antibodies. White arrowheads indicate the positions of the respective GST-tagged proteins.

Positively charged arginines in the amphipathic alpha helix mediate PM association and CML12/TCH3 binding

It has been reported that positively charged amino acids in the binding domains are crucial for interaction with CaM/CMLs (O'Neil and DeGrado., 1990; Clore et al., 1993; Arazi et al., 1995; Xu et al., 2012). To identify the key amino acids that are responsible for CaM/CML binding, we generated PID mutant versions in which some of the arginines that make up the amphipathic alpha helix in the PD ID were substituted with alanines (i.e. PID(R3)A, PID(R2A) and PID (R5A), see Figure 5A). *In vitro* pull-downs and BiFC assays showed that all three PID mutant versions cannot interact with CML12/TCH3 anymore (Figure 5B, C). Expression of these mutant versions in Arabidopsis protoplasts showed that their PM association was disrupted as they showed predominant cytosolic localization (Figure 5D).

These results indicated that the positively charged arginines in the predicted amphipathic alpha helix are vital for both PM association and CML12/TCH3 binding.

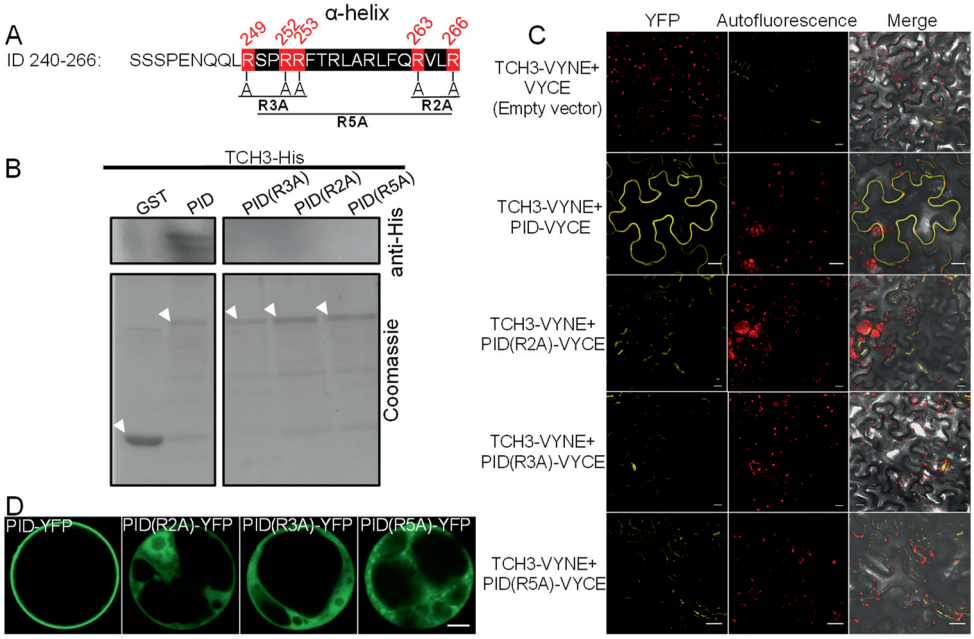

Figure 5. Positively charged arginines in the amphipathic alpha helix in the PID ID are essential for PM association and CaM/CML binding. (A). The amino acid sequence of the central part of the

PID ID, with the predicted amphipathic alpha helix indicated with white letters on a black background. The alanine substituted arginines are indicated in red, and the three PID mutant versions PID(R3A), PID(R2A) and PID(R5A) are indicated below the sequence. **(B)** *In vitro* pull-down using GST, GST-PID (PID), GST-PID(R2A), GST-PID(R3A) or GST-PID(R5A) (respectively PID(R2A), PID(R3A) or PID(R5A)) bound to glutathione beads as bait and His-tagged TCH3 as prey. Pulled down TCH3-His was detected by hybridizing the Western blot with anti-His antibodies (upper panel). White arrowheads indicate the positions of the respective GST-tagged proteins in a Coomassie stained gel (lower panel). **(C)** Bimolecular Fluorescence Complementation (BiFC) assay performed by transient *Agrobacterium*-mediated expression of the C-terminal half of YFP C-terminally fused to PID (PID - VYCE) or to the PID(R to A) mutants and the N-terminal half of YFP C-terminally fused to TCH3 (TCH3-VYNE) in leaf epidermis cells of three weeks old *Nicotiana benthamiana* plants. An empty vector expressing the N-terminal half of YFP (VYCE) was used as negative control. **(D)** Arabidopsis protoplasts transfected with *p35S:PID-YFP*, *p35S:PID(R2A)-YFP, p35S:PID(R3A)-YFP* or *p35S:PID(R5A)-YFP*. The scale bar in (**C**) and (**D**) indicates 10 µm.

Overexpression of arginine to alanine PID mutants show strong phenotypes resembling overexpression of wild type PID

By mapping the PM association and CaM/CML binding domains we aimed to separate these two activities in order to be able to generate an 'untouchable' PID version, which would overcome the anticipated functional redundancy among the 11 genes encoding PID interacting CaM/CMLs (see Chapter 2) and allow to study the role of the calcium-dependent regulation of PID activity. The above data suggests, however, that PM association and CaM/CML binding are tightly linked, as they converge at an amphipathic alpha helix in the PID ID. As PM association of PID was considered important for its role in phosphorylating PIN proteins (Dhonukshe et al., 2010), we set out to test the activity of the PID(R3A), PID(R2A) and PID(R5A) mutant versions by overexpressing them as YFP fusions in Arabidopsis.

Previously, we have shown that overexpression of wild-type *PID* causes strong seedling phenotypes, such as agravitropic root and shoot growth and collapse of the main root meristem. Moreover, flowering *PID* overexpression plants frequently develop pin-like inflorescences (Benjamins et al., 2001; Friml et al., 2004). Similar phenotypes were observed when we overexpressed a PID-YFP fusion in Arabidopsis (*p35S:PID-YFP*). Around 82% of the flowering T1 plants developed pin-like inflorescences (Figure 6A) and T3 seedlings of selected homozygous

single locus lines showed agravitropic growth and root meristem collapse (Figure 6B, D). Analysis of the root tips before meristem collapse by confocal microscopy showed clear PM association of the PID-YFP fusion protein (Figure 6D). Similar results were obtained for YFP fusions of PID versions in which part of the IQ-like motif was disrupted ((PID(K268A), PID(K269A), PID(K268,269A), PID(V270D) and PID(V270D/L273E)), which did not affect PM association or CML12/TCH3 binding (Figure S2A, B). Unexpectedly, overexpression of the three PID(R→A)-YFP fusions still resulted in a high percentage of T1 plants (between 72% and 86%) showing pin-like inflorescence (Figure 6A; Figure S2B). Moreover, T3 seedlings of selected homozygous single locus lines showed agravitropic growth and root meristem collapse (Figure 6B; Figure S2A). The severity of agavitropic growth and the occurrence of root meristem collapse corresponded to the level of overexpression in each line (Figure 6I). As observed in Arabidopsis protoplasts (Figure 5D), the PID(R3A), PID(R2A) and PID(R5A) versions showed predominant cytosolic localization in root tip cells (Figure 6F, H). Taken together, these results suggest that the three PID(R→A) versions are still functional kinases despite their predominant cytosolic localisation.

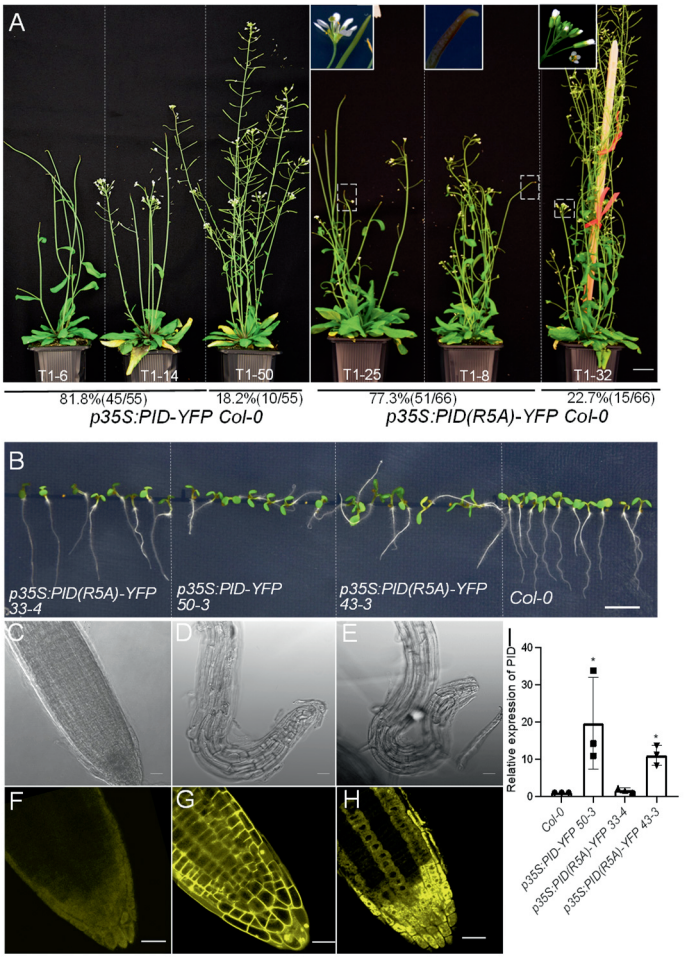

Figure 6. Overexpression studies indicate that PID(R5A) is a functional kinase. (**A**) Phenotypes of flowering T1 plants transgenic for *p35S:PID-YFP* or *p35S:PID(R5A)-YFP*. Below the percentage and number of T1 plants showing pin-like or wild-type inflorescences are indicated. (**B**) Phenotype of 5-day-old vertically grown seedlings of wild-type Arabidopsis (Col-0) or of selected *p35S:PID-YFP* and *p35S:PID(R5A)-YFP* T3 lines. **(C-E**). Root tip phenotype of a weak expressing *p35S:PID(R5A)-YFP* seedling (**C**) or of a strong expressing *p35S:PID-YFP* (**D**) or *p35S:PID(R5A)-YFP* (**E**) seedling in (**B**). **(F-H**). Representative confocal images showing YFP signal in the root tips of *35S:PID-YFP* and *35S:PID(R5A)-YFP* seedlings in (**B**). (**I**) Relative expression levels of PID, as determined by qRT-PCR analysis on RNA isolated from the seedlings of the indicated lines presented in (**B**). Different dots indicate the values of three biological replicates per plant line, bar indicates the mean, and error bars indicate the SEM. The asterisk indicates a significant difference from wild type ($P < 0.05$), as determined by Student's *t*-test. Size bars indicate 2 cm in (A), 1 cm in (B), 20 um in (C-H).

Complementation of *pid* loss-of-function mutant defects by PID(R→A) versions confirms their functionality.

To further validate the kinase activity of the PID(R→A) versions, we generated *pPID:PID-YFP* and *pPID:PID(R→A)-YFP* fusion constructs and transformed those to plants heterozygous for the strong *pid-14* loss-of-function mutant allele. T1 plants homozygous for the *pid-14* allele were selected for phenotyping (Figure 7A). The wild-type *pPID:PID-YFP* construct fully restored the severe shoot defects of *pid-14* in 12 of the 14 (85,7%) selected T1 plants, whereas two T1 plants showed incomplete rescue as they still developed pin-like inflorescences (Figure 7A, B). For the *pPID:PID(RtoA)-YFP* constructs a similar percentage of T1 plants (75, 88 or 80%, respectively) showed full rescue of the mutant phenotype (Figure 7A, B). These results confirm the conclusions from the overexpression experiments that the PID(R→A) mutant versions are still functional despite their loss of PM association. On the one hand, this implies that the PM association of PID, unlike what was previously assumed (Dhonukshe et al., 2010), is not essential for its function. This suggests that the key effect of the calcium-dependent binding of CaM/CMLs to PID is the reduced kinase activity rather than the sequestration from the PM. On the other hand, we can conclude that with the PID(R→A) versions we have generated the desired 'untouchable' PID mutants and that the *pPID:PID(RtoA)-YFP pid-14* lines now should give us the possibility to identify the role of the PID-CaM/CMLs complex in plants growth and development.

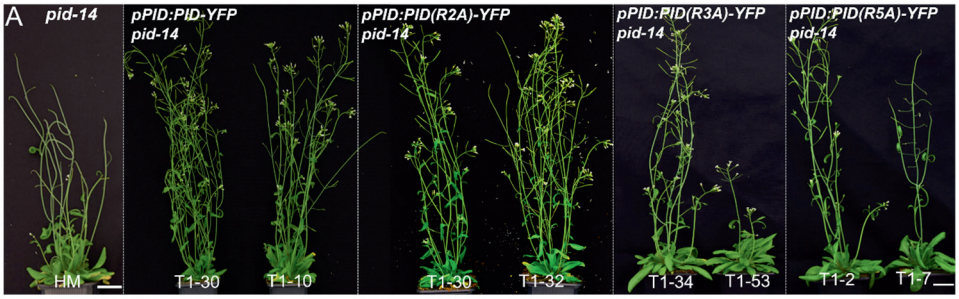

B

Constructs	T1 plants (*pid-14* HM)	Inflorescence	
		WT-like	pin-like
pPID:PID-YFP pid-14	14	85.7%(12/14)	14.3%(2/14)
pPID:PID(R3A)-YFP pid-14	16	75.0%(12/16)	25.0%(4/16)
pPID:PID(R2A)-YFP pid-14	25	88.0%(22/25)	12.0%(3/25)
pPID:PID(R5A)-YFP pid-14	15	80.0%(12/15)	20.0%(3/15)

Figure 7. PID(R→A) variants complement the *pid-14* mutant inflorescence defects. (A) Flowering plants phenotypes of the *pid-14* mutant and of selected *pPID:PID-YFP pid-14*, *pPID:PID(R2A)-YFP pid-14*, *pPID:PID(R3A)-YFP pid-14, pPID:PID(R5A)-YFP pid-14* T1 plants. Size bar indicates 2 cm in (A). (**B**). Table depicting the total number of T1 plants homozygous for the *pid-14* allele (*pid-14* HM) that were used for phenotyping, and the number and percentage of T1 plants showing either a wild-type-like (WT-like) or a pin-like inflorescence phenotype.

Discussion

Ca^{2+} signalling has for a long time been reported to play a role in the action of the plant hormone auxin, in part by regulating its polar cell-to-cell transport (Dela Fuente and Leopold, 1973; Dela Fuente, 1984). The serine/threonine kinase PID also regulates PAT by phosphorylating the PIN auxin efflux carriers and thereby directing their polarity and enhancing their activity (Friml et al., 2004, Huang et al., 2010; Dhonukshe et al., 2010; Zourelidou et al., 2014). The finding that the calcium binding proteins CML12/TCH3 and PBP1 interact with PID and regulate its kinase activity *in vitro* provided the first molecular link between Ca^{2+} signalling and PAT (Benjamins et al., 2003). Auxin-induced and calcium-dependent binding of CML12/TCH3 reduced the kinase activity of PID *in vitro* and sequestered PID from the PM to the cytosol in Arabidopsis protoplasts and root and shoot epidermal

cells (Galvan-Ampudia, 2009; Fan, 2014; Chapter 2). Our study in Chapter 2 of this thesis showed that, besides CML12/TCH3, the closely related three CMLs (CML8, CML10, CML11) and all seven Arabidopsis CaMs act redundantly in binding PID. The genes encoding these PID interacting CaM/CMLs share a largely overlapping expression pattern, and single *cam/cml* T-DNA insertion mutants we did not see a phenotype distinguishable from wild-type Arabidopsis. Therefore, to overcome the likely functional redundancy of these PID interacting CaM/CML genes in our attempt to reveal the role of the PID-CaM/CML interaction in plant development, we mapped the CaM/CMLs binding domain in PID. This resulted in the identification of an amphipathic alpha helix in the PID insertion domain that mediates both PM association and CaM/CML binding. Disruption of this amphipathic alpha helix by substituting some of the positively charged arginines to alanins resulted in PID(R→A) mutant versions that were no longer PM associated and did not interact with CaM/CMLs anymore, but were still functional based on overexpression phenotypes and complementation of the *pid* loss-of-function mutant. In Chapter 4 of this thesis, these 'untouchable' PID mutant versions are used to investigate the role of the PID-CaM/CML interaction in plant growth and development.

CaM/CML binding and PM association domain converge on an amphipathic alpha helix in the PID ID

Our results show that both PM association and CaM/CML binding converge at an amphipathic alpha helix in the ID located in the middle of the catalytic core of the PID kinase. Previous research has already shown that CaM/CMLs do bind to amphipathic alpha helices with high affinity and broad specificity (O'Neil and DeGrado, 1990), and that this structural feature is frequently found in CaM/CML binding proteins (Persechini and Kretsinger, 1988; O'Neil and DeGrado, 1990; Crivici and Ikura, 1995; Komolov et al., 2021). In our case, the identified amphipathic alpha helix has seven positively charged amino acids on one side, and

six hydrophobic amino acids on the other side, which is perfectly in accordance with the features previously described for such an alpha helix (O'Neil and DeGrado, 1990).

Interestingly, we also identified an IQ-like motif in the PID ID that partially overlaps with the amphipathic alpha helix. The IQ/IQ-like motif was identified using the consensus sequences that were based on a large group of calmodulin binding proteins, including unconventional myosins (Bähler and Rhoads, 2002), ion channels (sodium, potassium, calcium channels and etc.) (Schumacher et al., 2004; Fallon et al., 2005; Mori et al., 2008; Fallon et al., 2009; Reddy Sarhan et al., 2012; Wang et al., 2012; Chichili et al., 2013) and PM Ca^{2+}-ATPases (Tidow et al., 2012). It has been reported for several animal proteins, including utrophin, Ras guanine nucleotide-releasing factor, Nina C myosins and calcium vector target protein, that CaM/CMLs can bind to IQ-motifs in a calcium-dependent manner (Bähler and Rhoads, 2002). But exceptions were also found, for example, some CaMs or CaM-related proteins serve as myosin light chains to interact with the IQ domains of myosin independently of Ca^{2+} (Cheney and Mooseker, 1992; Atcheson et al., 2011; Heissler and Sellers, 2014). The IQ-like motif is similar to the IQ-motif, but can bind to a broader range of proteins in a calcium-dependent manner (Houdusse and Cohen, 1995). The IQ-like motif we identified in the PID ID lacks the conserved central G residue and the second basic residues. Substitution of some positively charged or hydrophobic amino acids in this IQ-like motif did not affect CML12/TCH3 binding or the function of PID based on overexpression phenotypes and complementation of the *pid* loss-of-function mutant. In addition, the central segment PID ID $_{240\text{-}266}$, in which the C-terminal part of the IQ-like motif was lacking, could still interact with CML12/TCH3. These data suggest that this putative IQ-like motif is not involved in binding with CaM/CMLs.

Results by Zegzouti and co-authors (2006) already indicated that the PID ID is involved in PM association of the kinase. Our results confirmed this and are in line with a more recent report on the interactions of the positive arginine residues in the

PID ID with the negative electrostatic field generated especially by the phosphatidylinositol-4-phosphate (PI4P)-enriched PM (Simon et al., 2016). These negative charges in the PM contribute to the localization of many proteins containing polybasic clusters or cationic domains through electrostatic interactions (Heo et al., 2006; McLaughlin and Murray, 2005). This supports our findings that the amphipathic alpha helix in the PID ID has a positively charged face and that the arginine residues responsible for this positive charge are crucial for the electrostatic association of PID with the PM. These findings are also in line with the observation that the mutant version PID(R/K9Q), in which all nine positively charged amino acids (arginines and lysines) in the PID $ID_{248-270}$ are substituted by the uncharged glutamine (Q), does not associate anymore with the PM (Simon et al., 2016).

The dual role of the amphipathic alpha helix in the PID ID also explains why CaM/CMLs sequestrate PID from the PM to the cytosol. CaM/CML binding is likely to shield the positively charged arginines in the amphipathic alpha helix from the negatively charged PM and thereby prevent PM association. According to previous studies, CaM/CMLs have a much higher affinity to target proteins when the EF-hands are occupied with Ca^{2+} than the lipid biolayer, but this situation is reversed in the absence of Ca^{2+} (Gillette et al., 2015; Agamasu et al., 2019; Grant et al., 2020).

Predominant PM association is not important for PID function

PID is known as a protein kinase that localizes predominantly at the PM of epidermis cells in the embryo, root tip (including root hairs) and the shoot apical meristem (Lee and Cho, 2006; Michniewicz et al., 2007; Dhonukshe et al., 2010; Landrein et al., 2015; Simon et al., 2016) and in Arabidopsis protoplasts (Galvan-Ampudia, 2009; Chapter 2). The PM association of PID makes sense in view of its role as regulator of PIN polarity by direct phosphorylation of these auxin efflux carriers (Friml et al., 2004; Huang et al., 2010; Dhonukshe et al., 2010; Zourelidou

et al., 2014). However, PID localization is dynamic, as it has also been observed localized to the cytoplasm and some subcellular compartments, indicating that it cycles between the PM and the cytoplasm or intracellular compartments. Treatments with brefeldin A (BFA), which targets GNOM-mediated basal PIN recycling, the kinase inhibitor staurosporine (ST), NaCl or the PI4-kinase (PI4K) inhibitor phenylarsine oxide (PAO) all cause strong PID internalization from the PM to the cytosol (Lee and Cho, 2006; Dhonukshe et al., 2010; Simon et al., 2016; Wang et al., 2019). Our data show that auxin can induce internalization of PID in a Ca^{2+}-dependent manner in epidermis cells in the root tip and shoot meristem and in Arabidopsis protoplasts (Galvan-Ampudia, 2009; Fan, 2014; Chapter 2) and that abiotic signals such as gravity and mechanical stress are also able to cause the internalization of PID (Fan, 2014). The latter makes sense in view of the PID-CaM/CML interaction, since both auxin and abiotic signals cause elevations in the $[Ca^{2+}]_{cyt}$.

However, our results on the activity of the 'untouchable' PID versions suggest that its PM localization is not important for its activity. This implies that recruitment of PID from the PM by the CaM/CML interaction is rather a side effect, and that reduced activity or inactivation of the kinase by CaM/CML binding is more important. This is seemingly in contrast to a previous report, showing that inhibition of PID activity by the kinase inhibitors staurosporine (ST) restores the root hair growth in *PID* overexpression lines, but that PID localization at the PM is disrupted and that the kinase is internalized to the cytosol (Lee and Cho, 2006). In the same publication also shown that overexpression of the kinase dead PID(D225G) or PID(D205N) mutant versions (Christensen et al., 2000) has no inhibitory effect on root hair growth and that the mutant proteins show largely dispersed cytoplasmic distribution (Lee and Cho, 2006). These results indicate that kinase activity and PM association of PID are tightly linked. Recently, we have provided evidence that PID is in a complex at the PM with MACCHI-BOU 4/MAB4(ENP1)-LIKE (MAB4/MEL) and PIN proteins and that this complex is

self-reinforced by PID-mediated PIN phosphorylation (Glanc et al., 2021). The formation of this complex could be important to initiate PID PM localization and require PID activity (hence the cytosolic localization of kinase dead versions), whereas the amphipathic alpha helix in the PID ID would be subsequently needed to maintain PM localization for a longer period. This model would also explain why our PID(R→A) versions, despite their cytosolic localization, are not disrupted in their activity, as their short term/transient recruitment to the PM localized PIN phospho-targets would still be promoted by the MAB4/MEL scaffold proteins. The above model explains that predominant PM association is not essential for PID function, which is corroborated by or observation that PID(R→A) versions do not need higher expression levels to induce overexpression phenotypes or complement *pid* loss-of-function defects compared to wild-type PID.

Material and Methods

Molecular cloning and constructs

The constructs *pDEST-PID-VYCE, pDEST-TCH3-VYNE, pET16H-TCH3*, *pGEX-PID*, *pART7-TCH3-CFP*, *pART7-PID-YFP*, *pDONR-PID* are described in Chapter 2.

For construct *pDONR207-PID(–ID)*, the entire *pDONR-PID* plasmid excluding the ID (AA 227 to 280) segment, but including the rest of the PID cDNA and the vector backbone was amplified using primers *PID Deletion 2 S* and *PID Deletion 2 AS* (Table S1). The PCR product was digested with *Bsp*TI and self-ligated, yielding *pDONR207-PID(–ID).*

For construct *pDONR207-PID(+ID)*, the ID was amplified using primers PID InsDom S and PID InsDom AS (Table S1), the resulting fragment was digested with *Sgs*I and *Bsp*TI and inserted by ligation into *pDONR207-PID(–ID)* digested with *Sgs*I and *Bsp*TI .

For construct *pDONR207-PID(+ID*$_{227\text{-}253}$*)*, *pDONR207-PID(+ID*$_{240\text{-}266}$*)* and *pDONR207-PID(+ID*$_{254\text{-}280}$*)*, DNA fragments coding for the ID segments 227-253, 240-266 and 254-280 with *Sgs*I and *Bsp*TI restriction sites added were generated by annealing the corresponding oligonucleotides indicated in Table S1, following the protocol from Sigma-Aldrich. The resulting fragments were digested with *Sgs*I and *Bsp*TI and inserted by ligation into *pDONR207-PID(-ID)* digested with *Sgs*I and *Bsp*TI.

The constructs *pDONR207-PID(Ala1), pDONR207-PID(Ala2)*, *pDONR207-PID(Ala3) pDONR-PID(R2A), pDONR-PID(R3A), pDONR-PID(R5A), pDONR-PID(K268A), pDONR-PID(K269A), pDONR-PID(K268,269A), pDONR-PID(V270D), pDONR-PID(V270D/L273E)* were obtained using the Agilent QuickChange II XL site directed mutagenesis kit and the corresponding primer sets listed in Table S1 with *pDONR-PID* or *pDONR-PID(R3A)* (for *pDONR-PID(R5A)*) as template.

The constructs *pDEST-PID(R2A)-VYCE, pDEST-PID(R3A)-VYCE, pDEST-PID(R5A)-VYCE* were obtained by recombining the coding region from the corresponding *pDONR* plasmid (see above) by LR reaction into *pDEST-^{GW}VYCE.*

For the binary plasmids *p35S:PID-YFP*, *p35S:PID(R2A)-YFP*, *p35S:PID(R3A)-YFP*, *p35S:PID(R5A)-YFP*, *p35S:PID(K268A)-YFP*, *p35S:PID(K269A)-YFP*, *p35S:PID(K268,269A)-YFP*, *p35S:PID(V270D)-YFP* and *p35S:PID(V270D/L273E)-YFP*, the corresponding coding region was first recombined by LR reaction from the *pDONR* plasmid (see above) into the *pART7-p35S-Gateway-YFP* Entry plasmid (Galvan-Ampudia, 2009). Subsequently, the *p35S:PID-YFP* expression cassette was ligated as *Not*I fragment in the T-region of the *Not*I digested binary vector *pART27* (Gleave, 1992).

The constructs *pPID:PID-YFP*, *pPID:PID(R2A)-YFP*, *pPID:PID(R3A)-YFP*, *pPID:PID(R5A)-YFP*, *pPID:PID(K268A)-YFP*, *pPID:PID(K269A)-YFP*, *pPID:PID (K268,269A)-YFP*, *pPID:PID(*V270D)-*YFP* and *pPID:PID(V270D/L273E)-YFP* were obtained by recombining the coding region by LR reaction from the corresponding *pDONR207* vector (see above) to *pGreenII0179 PID3.2kb::Gateway-YFP-HA* (Galvan-Ampudia, 2009).

Primers used were designed with CLC Main Workbench (CLC bio) software and listed in the Table S1.

Plant material, growth conditions and phenotype analysis

All *Arabidopsis thaliana* transgenic lines and mutants used in this study are in the Columbia (Col-0) background.

For Arabidopsis transgenic lines the binary plasmids *p35S:PID-YFP*, *p35S:PID(R2A)-YFP*, *p35S:PID(R3A)-YFP*, *p35S:PID(R5A)-YFP*, *p35S:PID(K268A)-YFP*, *p35S:PID(K269A)-YFP*, *p35S:PID(K268,269A)-YFP*, *p35S:PID(V270D)-YFP* and *p35S:PID(V270D/L273E)-YFP* were electroporated into Agrobacterium strain AGL1 (Lazo et al., 1991; Chassy et al., 1988) and T-DNA constructs were transformed to Col-0 using the floral dip method (Clough

and Bent., 1998). Primary transformants (T1) were selected on 0.5× Murashige and Skoog (1/2 MS) medium (Duchefa) containing 0.05% MES, 0.8% Daishin agar (Duchefa) and 1% sucrose, supplemented with 50 µg/ml kanamycin the constructs and with 100 µg/ml timentin to inhibit Agrobacterium growth, and the phenotypes were recorded. Single locus insertion and homozygous lines were used for further analysis.

Binary plasmids *pPID:PID-YFP*, *pPID:PID(R2A)-YFP*, *pPID:PID(R3A)-YFP*, *pPID:PID(R5A)-YFP*, *pPID:PID(K268A)-YFP*, *pPID:PID(K269A)-YFP*, *pPID:PID(K268,269A)-YFP*, *pPID:PID(V270D)-YFP* and *pPID:PID(V270D/L273E)-YFP* were electroporated into Agrobacterium strain AGL1 (Lazo et al., 1991; Chassy et al., 1988) and T-DNA constructs were transformed to heterozygous *pid-14/+ (Salk_049736)* plants using the floral dip method (Clough and Bent., 1998). Primary transformants (T1) were selected on medium supplemented with 25 µg/ml hygromycin for the constructs, 50 µg/ml kanamycin for the *pid-14* mutant allele and 100 µg/ml timentin to inhibit Agrobacterium growth. Homozygous *pid-14* plants were selected by genotyping with primers *PID LP* and *LBb1.3* (for SALK lines) and subsequently used for phenotyping. T3 lines with single locus homozygous T-DNA insertion were used for further analysis.

Seeds were surface sterilized by incubating for 1 min. in 70% ethanol and 10 min. in bleach solution containing 1% chlorine and subsequently washed three times with sterile dH_2O. Sterilized seeds were kept in the dark at 4 °C for two days for vernalization and subsequently germinated on vertical plates containing 0.5× Murashige and Skoog (1/2 MS) Duchefa medium containing 0.05% MES, 1% Daishin agar (Duchefa) and 1% sucrose at 22 °C and 16 hours photoperiod. Plants grown on soil were cultured at 21 °C, 16 hours photoperiod, and 70% relative humidity.

Seedlings on plates, potted plants were photographed with a Nikon D5300 camera. Primary root length was measured with ImageJ (Fiji) and analysed with GraphPad Prism 5.

Protein structure prediction and helix wheel projection

The structure of the PID ID was analysed by web protein structure prediction tools http://zhanglab.ccmb.med.umich.edu/QUARK/ (Xu and Zhang, 2012; Mortuza et al., 2021) and http://bioserv.rpbs.univ-paris-diderot.fr/PEP-FOLD/ (Thevenet et al., 2012; Shen et al., 2014). The helix wheel projection was made by http://heliquest.ipmc.cnrs.fr/. The consensus sequences for an IQ motif ([FILV]Qxxx[RK]Gxxx[RK]xx[FILVWY]) or an IQ-like motif ([FILV]Qxxx[RK]xxxxxxxx) were used to identify such a motif in PID.

RNA extraction and (q)RT-PCR

Vertically grown 5-day-old seedlings were collected and total RNA was extracted using the NucleoSpin RNA Plant kit (Macherey Nagel, #740949). Reverse transcription (RT) was performed using the RevertAid Reverse Transcription Kit (Thermo Scientific™, #K1691). qRT-PCR was performed in the CFX96 Touch™ Real-Time PCR Detection System (Bio-Rad) using TB Green® Premix Ex Taq™ II (Tli RNase H Plus) (Takara, #RR820B).

Protoplast transformation

Protoplasts of *Arabidopsis thaliana* Col-0 cell suspension cultures were obtained and transfected as described (Schirawski et al., 2000). Plasmid DNAs were extracted using the Plasmid Midi Kit (QIAGEN, #12143), 10µg per plasmid was added to 0.5×10^6 cells for PEG-mediated protoplast transfection. Auxin (NAA, 1 µM) was removed from the media during protoplast isolation and transfection, and either left out or added to the recovery medium after transfection. The transfected protoplasts were incubated for 16 hours at 21 °C in the dark. Pictures were taken

using the Zeiss LSM5 Exciter/Axio Observer confocal microscope with either a 40x or 63x oil immersion objective (NA=1.2). The CFP signal was detected using an argon 458 nm laser and a 475-525 nm band pass filter, and the YFP signal was detected using an argon 514 nm laser and a 530-600 nm band pass filter.

In vitro pull-down assay

In vitro pull-down assays were performed as described in Chapter 2.

Bimolecular Fluorescence Complementation (BiFC) assay

To perform the BiFC assays, 20 ml cultures of *Agrobacterium tumefaciens* strain AGL1 harbouring either *pDEST–PID-VYCE, pDEST–PID(R2A)-VYCE, pDEST–PID(R3A)-VYCE, pDEST–PID(R5A)-VYCE, pDEST–TCH3/CML12*-VYNE or *pDEST-VYCE* were incubated in a 28°C shaker until an OD_{600} of 1.0 was reached. Bacteria were collected by centrifugation for 15 minutes at 4000rpm, resuspended in 20 ml infiltration medium (10 mM $MgCl_2$, 10 mM MES/KOH, pH 5.7) supplemented with 200µM Acetosyringone (Sigma-Aldrich, #D134406-5G), and cultured for at least 2 hours at 50 rpm on a table shaker in darkness. Equal volumes of the agrobacteria carrying two constructs (5 ml each) were mixed. Leaves of three-week-old *Nicotiana benthamiana* plants were infiltrated using a 5 ml syringe without needle. Two days later, infiltrated leaf parts were checked for YFP signal using the Zeiss LSM 5 Exciter 2C/1F Imager M1 (Zeiss, Oberkochen, Germany) confocal microscope, using a 20x objective. The YFP signal was detected using an argon 514 nm laser and a 530-600 nm band pass filter.

Accession numbers

Arabidopsis Genome Initiative locus identifiers for the genes mentioned are as follows: CaM1/TCH1 (At5g37780), CaM2 (At2g41110), CaM3 (At3g56800), CaM4 (At1g66410), CaM5 (At2g27030), CaM6 (At5g21274), CaM7 (At3g43810),

CML8 (At4g14640), CML9 (At3g51920), CML10 (At2g41090), CML11 (At3g22930), CML12/TCH3 (At2g41100), PID (At2g34650).

Acknowledgements

The authors would like to thank Gerda Lamers and Joost Willemse for their help with the microscopy, Ward de Winter and Jan Vink for help with medium, tissue culture and plant caretaking. This author was supported by the China Scholarship Council.

Author contribution

Remko Offringa, Xiaoyu Wei designed the experiments, Yuanwei Fan and Eike Rademacher performed experiments presented Figure 1-4 and figure 5 (A, B, D), Xiaoyu Wei performed the rest of the experiments and data analysis, Xiaoyu Wei and Remko Offringa wrote and finalized of the Chapter.

Supplementary data:

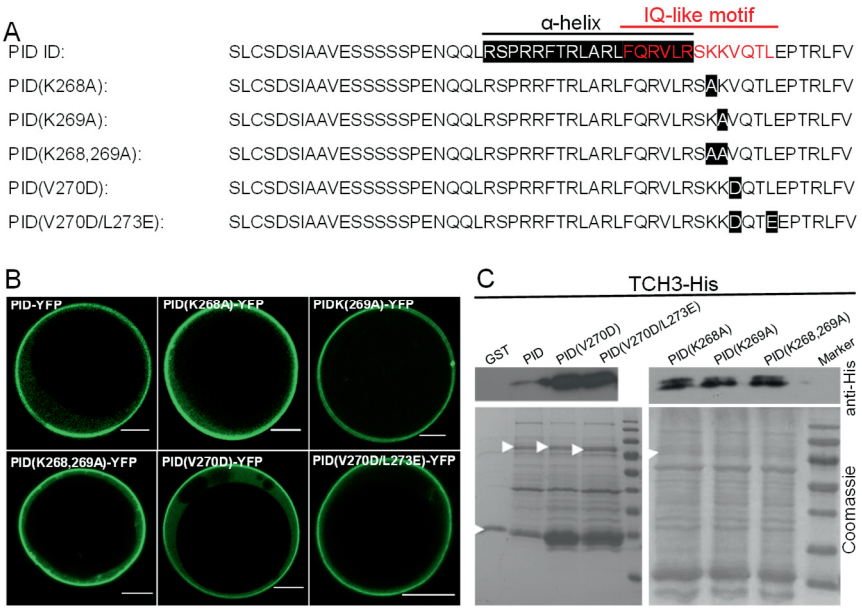

Figure S1. Disruption of the IQ-like motif does affect either PM association or CaM/CML binding. (**A**). The amino acid sequence of PID ID and the amino acid substitutions in different PID mutant versions. (**B**). Expression of PID-YFP, PID(K268A)-YFP, PID(K269A)-YFP, PID(K268,269A)-YFP, PID(V270D)-YFP or PID(V270D/L273E)-YFP fusions from the *35S* promoter in Arabidopsis protoplasts. (**C**) *In vitro* pull down using GST, GST-tagged PID (PID) or GST-tagged PID mutant versions PID(K268A), PID(K269A), PID(K268,269A), PID(V270D), PID(V270D/L273E) bound to glutathione beads as bait and His-tagged TCH3 as prey. Pulled down TCH3-His was detected by hybridizing the Western blot with anti-His antibodies (upper panel). White arrowheads in lower panel indicate the positions of the respective GST-tagged proteins in a Coomassie stained gel. The scale bar in (**B**) indicates 10 µm.

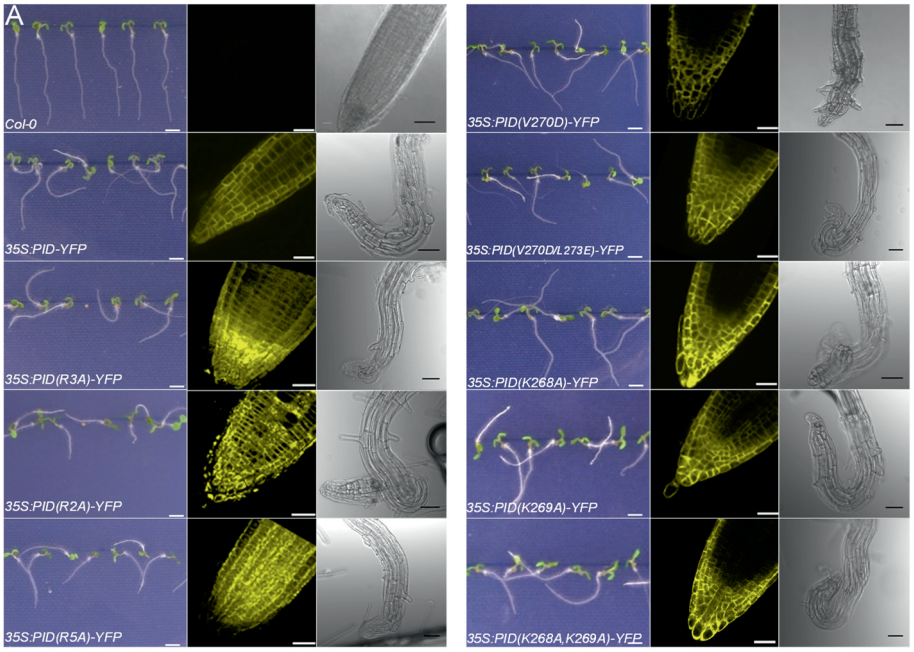

B

Constructs	T1 plants (*Col-0*)	Inflorescence	
		pin-like	WT-like
p35S:PID-YFP	55	81.8%(45/55)	18.2%(10/55)
p35S:PID(V270D)-YFP	23	78.3%(18/23)	21.7%(5/23)
p35S:PID(V270D/L273E)-YFP	9	88.9%(8/9)	11.1%(1/9)
p35S:PID(K268A)-YFP	28	75.0%(21/28)	25.0%(7/28)
p35S:PID(K269A)-YFP	24	83.3%(20/24)	16.7%(4/24)
p35S:PID(K268A,K269A)-YFP	24	79.2%(19/24)	20.8%(5/24)
p35S:PID(R3A)-YFP	29	72.4%(21/29)	27.6%(8/29)
p35S:PID(R2A)-YFP	36	86.1%(31/36)	13.9%(5/36)
p35S:PID(R5A)-YFP	66	77.3%(51/66)	22.7%(15/66)

Figure S2. Seedling phenotypes of lines overexpressing wild-type PID or mutant PID versions. (A). Phenotype of 5-day-old vertically grown seedlings (left image) and confocal microscopy analysis of the root tip showing the YFP signal (middle image) or the transmitted light (right image) of wild-type Arabidopsis (Col-0) or of T3 lines homozygous for a single locus insertion of the *p35S:PID-YFP, p35S:PID(R2A)-YFP, p35S:PID(R3A)-YFP, p35S:PID(R5A)-YFP, p35S:PID(K268A)-YFP,*

p35S:PID(K269A)-YFP, *p35S:PID(K268A,K269A)-YFP*, *p35S:PID(V270D)-YFP* or *p35S:PID(V270D/L273E)-YFP* T-DNA construct. **(B).** Table depicting the number of primary transformants (T1) phenotyped at the flowering plant level and the number and percentage of plants developing either wild-type or pin-like inflorescences. Size bar indicates 0.2 cm in the left panel, 20 µm in the middle panel and 50 µm in the right panel of **(A)**.

A

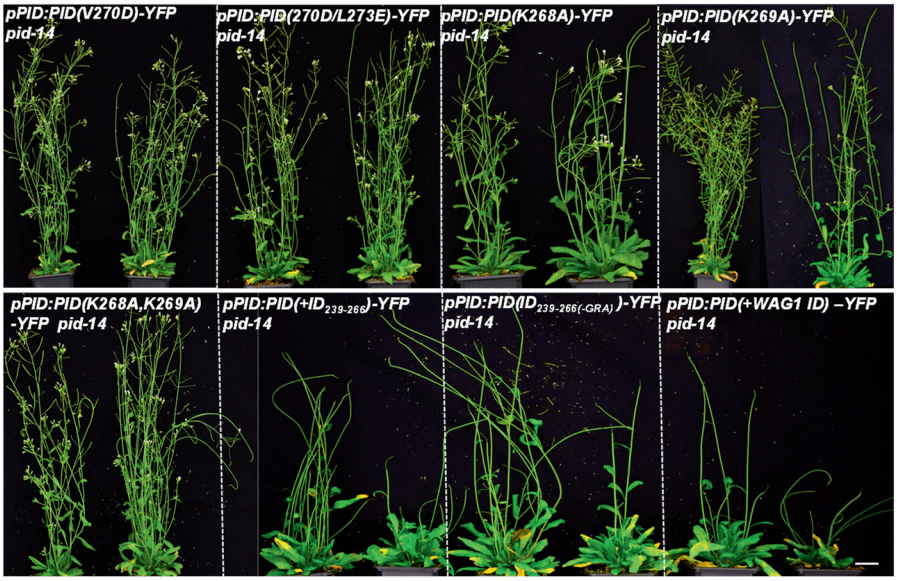

B

Constructs	T1 plants (*pid-14 HM*)	Inflorescence	
		WT	pin-like
pPID:PID-YFP pid-14	14	85.7%(12/14)	14.3%(2/14)
pPID:PID(V270D)-YFP pid-14	15	80.0%(12/15)	20.0%(3/15)
pPID:PID(V270D/L273E)-YFP pid-14	17	94.1%(16/17)	5.9%(1/17)
pPID:PID(K268A)-YFP pid-14	10	80.0%(8/10)	20.0%(2/10)
pPID:PID(K269A)-YFP pid-14	14	85.7%(12/14)	14.3%(2/14)
pPID:PID(K268A,K269A)-YFP pid-14	9	77.8%(7/9)	22.2%(2/9)
pPID:PID(+ID$_{239-266}$)-YFP pid-14	31	19.4%(6/31)	80.6%(25/31)
pPID:PID(ID$_{239-266(-GRA)}$)-YFP pid-14	6	16.7%%(1/6)	83.3%(5/6)
pPID:PID(+WAG1 ID) –YFP pid-14	17	0.0%(0/17)	100%(17/17)

Figure S3. Complementation analysis of mutant PID versions expressed under the *PID* promoter in the *pid-14* mutant background. (**A**) Flowering plant phenotype of primary transformants (T1) homozygous for the *pid-14* loss-of-function allele and transgenic for the

pPID:PID-YFP, *pPID:PID(R2A)-YFP*, *pPID:PID(R3A)-YFP*, *pPID:PID(R5A)-YFP*, *pPID:PID(K268A)-YFP*, *pPID:PID(K269A)-YFP*, *pPID:PID(K268A,K269A)-YFP*, *pPID:PID(V270D)-YFP*, *pPID:PID(V270D/L273E)-YFP*. (**B**). Table depicting the number of phenotyped primary transformants (T1) with the indicated T-DNA construct and homozygous for the *pid-14* allele (*pid-14* HM), and the number and percentage of transformants showing wild-type or pin-like inflorescences. Size bar indicates 2 cm in **(A).**

Table S1. Oligonucleotides used for cloning, genotyping or qRT-PCR.

AttB1 InsDom AA229 S	5'GGGGACAAGTTTGTACAAAAAAGCAGGCTTAATGCTATGCTCCGACTCAATCG3'
AttB2 InsDom AA279 AS	5'GGGGACCACTTTGTACAAGAAAGCTGGGTCAAAGAGACGGGTTGG3'
AttB1 InsDom AA248 S	5'GGGGACAAGTTTGTACAAAAAAGCAGGCTTAATGGAGAATCAACAACTC3'
AttB2 InsDom AA274 AS	5'GGGGACCACTTTGTACAAGAAAGCTGGGTGTTCTAAAGTCTGAACC3'
PID Deletion 2 S	***Bsp*TI** *Sgs*I 5'AAA**CTTAAG**GGCGCGCCCGAGGTCAAAGTCAGAGAGC3'
PID Deletion 2 AS	***Bsp*TI** 5'GAC**CTTAAG**GCTGAACCGGTTACTGC3'
PID InsDom S	*Sgs*I 5'TGGCGCGCCTCTCTATGCTCCGACTCAAT3'
PID InsDom AS	***Bsp*TI** 5'CGT**CTTAAG**AACAAAGAGACGGGTTGG3'
PID InsDom R249,252,253A AS	5'GTGAATGCTGCAGGTGAAGCGAGTTGTTG 3'
PID InsDom R263,266A	5'CTTTTCCAAGCAGTACTGGCGTCTAAAAAGG3'
PID InsDom R268A	5'TCCAACGAGTCTTGCGGTCTGCAAAGGTTCAGACTTTAGAAC3'
PID InsDom R269A	5'GGTTGGTTCTAAAGTCTGAACAGCTTTAGACCGCAAGACTCGTTGG3'
PID InsDom R268,269A	5'GACGGGTTGGTTCTAAAGTCTGAACAGCTGCAGACCGCAAGACTCGTTGGAAAAGT3'
PID-ALA1 S	5'GAATCTTCCTCGTCTTCGCCGGAGAATCAAGCAGCCGCTGCAGCGGCAGCATTC ACTCGTCTCGCTAGACTTTTCCAACG3'
PID-ALA1 AS	5'CGTTGGAAAAGTCTAGCGAGACGAGTGAATGCTGCCGCTGCAGCGGCTGCTTGA TTCTCCGGCGAAGACGAGGAAGATTC3'
PID-ALA2 S	5'GAGAATCAACAACTCCGTTCACCGCGACGAGCCGCTGCTGCCGCTGCAGCTTTC CAACGAGTCTTGCGGTCTAAAAAGGT3'
PID-ALA2 AS	5'ACCTTTTTAGACCGCAAGACTCGTTGGAAAGCTGCAGCGGCAGCAGCGGCTCGT CGCGGTGAACGGAGTTGTTGATTCTC3'
PID-ALA3 S	5'CACCGCGACGATTCACTCGTCTCGCTAGACTTGCCGCAGCAGCCGCGGCGGCTA AAAAGGTTCAGACTTTAGAACCAACCCGT3'
PID-ALA3 AS	5'ACGGGTTGGTTCTAAAGTCTGAACCTTTTTAGCCGCCGCGGCTGCTGCGGCAAGT CTAGCGAGACGAGTGAATCGTCGCGGTG3'
PID InsDom AA227-253 S	5'CGCGCCTCTCTATGCTCCGACTCAATCGCAGCCGTTGAATCTTCCTCGTCTTCG CCGGAGAATCAACAACTCCGTTCACCGCGACGAC3'
PID InsDom AA227-253 AS	5'TTAAGTCGTCGCGGTGAACGGAGTTGTTGATTCTCCGGCGAAGACGAGGAAGATTCAACGGCTGC GATTGAGTCGGAGCATAGAGAGG3'
PID InsDom AA254-280 S	5'CGCGCCTTCACTCGTCTCGCTAGACTTTTCCAACGAGTCTTGCGGTCTAAAAA GGTTCAGACTTTAGAACCAACCCGTCTCTTTGTTC3'
PID InsDom AA254-280 AS	5'TTAAGAACAAAGAGACGGGTTGGTTCTAAAGTCTGAACCTTTTTAGACCGCA AGACTCGTTGGAAAAGTCTAGCGAGACGAGTGAAGG3'
PID InsDom AA240-266 S	5'CGCGCCTCGTCTTCGCCGGAGAATCAACAACTCCGTTCACCGCGACGATTCA CTCGTCTCGCTAGACTTTTCCAACGAGTCTTGCGGC3'
PID InsDom AA240-266 AS	5'TTAAGCCGCAAGACTCGTTGGAAAAGTCTAGCGAGACGAGTGAATCGTCGCG

	GTGAACGGAGTTGTTGATTCTCCGGCGAAGACGAGG3’
PP2A-3-qRT-FP	5’GATGGATACAACTGGGCTCACG3’
PP2A-3-qRT-RP	5’TCGGTGCTGGTTCAAACTGG3’
PID-qRT-FP	5’ATTTACACTCTCTCCGTCATAGACAAC3’
PID -qRT-RP	5’ACATGTGTAGATATTCTAACGCCACTA3’
LBb1.3 (for SALK lines)	5’ATTTTGCCGATTTCGGAAC3’
PID LP	5’CTGTAACCAAAAACAAAATAAA3’

Reference:

Agamasu, C., Ghirlando, R., Taylor, T., Messing, S., Tran, T. H., Bindu, L., ... & Stephen, A. G. (2019). KRAS prenylation is required for bivalent binding with calmodulin in a nucleotide-independent manner. Biophys. J. 116: 1049-1063.

Andrews, C., Xu, Y., Kirberger, M., & Yang, J. J. (2020). Structural aspects and prediction of calmodulin-binding proteins. Int. J. Mol. Sci. 22: 308.

Arazi, T., Baum, G., Snedden, W. A., Shelp, B. J., & Fromm, H. (1995). Molecular and biochemical analysis of calmodulin interactions with the calmodulin-binding domain of plant glutamate **decarboxylase**. Plant Physiol. 108: 551-561.

Atcheson, E., Hamilton, E., Pathmanathan, S., Greer, B., Harriott, P., & Timson, D. J. (2011). IQ-motif selectivity in human IQGAP2 and IQGAP3: binding of calmodulin and myosin essential light chain. Biosci. Rep. 31: 371-379.

Babu, Y. S., Bugg, C. E., & Cook, W. J. (1988). Structure of calmodulin refined at 2.2 Å resolution. J. Mol. Biol. 204: 191-204.

Bähler, M., & Rhoads, A. (2002). Calmodulin signaling via the IQ motif. FEBS Lett. 513: 107-113.

Baum, G., Long, J. C., Jenkins, G. I., & Trewavas, A. J. (1999). Stimulation of the blue light phototropic receptor NPH1 causes a transient increase in cytosolic Ca^{2+}. Proc. Natl. Acad. Sci. U.S.A. 96: 13554-13559.

Benjamins, R., Quint, A., Weijers, D., Hooykaas, P., & Offringa, R. (2001). The PINOID protein kinase regulates organ development in Arabidopsis by enhancing polar auxin transport. Development 128: 4057-4067.

Black, D. J., & Persechini, A. (2011). In calmodulin–IQ domain complexes, the Ca^{2+}-free and Ca^{2+}-bound forms of the calmodulin C-lobe direct the N-lobe to different binding sites. Biochemistry 50: 10061-10068.

Chassy, B. M., Mercenier, A., & Flickinger, J. (1988). Transformation of bacteria by electroporation. Trends Biotechnol. 6: 303-309.

Chattopadhyaya, R., Meador, W. E., Means, A. R., & Quiocho, F. A. (1992). Calmodulin structure refined at 1.7 Å resolution. J. Mol. Biol. 228: 1177-1192.

Cheney, R. E., & Mooseker, M. S. (1992). Unconventional myosins. Curr. Opin. Cell Biol.

Chichili, V. P. R., Xiao, Y., Seetharaman, J., Cummins, T. R., & Sivaraman, J. (2013). Structural basis for the modulation of the neuronal voltage-gated sodium channel NaV1. 6 by calmodulin. Sci. Rep. 3: 2435.

Christensen, S. K., Dagenais, N., Chory, J., & Weigel, D. (2000). Regulation of auxin response by the protein kinase PINOID. Cell 100: 469-478.

Clore, G. M., Bax, A., Ikura, M., & Gronenborn, A. M. (1993). Structure of calmodulin-target peptide complexes: Curr. Opin. Struct. Biol. 3: 838–845.

Clough, S. J., & Bent, A. F. (1998). Floral dip: a simplified method for Agrobacterium-mediated transformation of Arabidopsis thaliana. Plant J. 16: 735-743.

Crivici, A., & Ikura, M. (1995). Molecular and structural basis of target recognition by calmodulin. Annu. Rev. Biophys. Biomol. Struct. 24: 85–116.

Davis, T. N., Urdea, M. S., Masiarz, F. R., & Thorner, J. (1986). Isolation of the yeast calmodulin gene: calmodulin is an essential protein. Cell 47: 423–431.

Dela Fuente, R. K. (1984). Role of calcium in the polar secretion of indoleacetic acid. Plant Physiol. 76: 342-346.

Dela Fuente, R. K., & Leopold, A. C. (1973). A role for calcium in auxin transport. Plant Physiol. 51: 845-847.

Dhonukshe, P., Huang, F., Galvan-Ampudia, C. S., Mähönen, A. P., Kleine-Vehn, J., Xu, J., ... & Offringa, R. (2010). Plasma membrane-bound AGC3 kinases phosphorylate PIN auxin carriers at TPRXS (N/S) motifs to direct apical PIN recycling. Development 137: 3245-3255.

Dindas, J., Scherzer, S., Roelfsema, M. R. G., von Meyer, K., Müller, H. M., Al-Rasheid, K. A. S., ... & Hedrich, R. (2018). AUX1-mediated root hair auxin influx governs SCFTIR1/AFB-type Ca^{2+} signaling. Nat. Commun. 9: 1174.

Fallon, J. L., Baker, M. R., Xiong, L., Loy, R. E., Yang, G., Dirksen, R. T., ... & Quiocho, F. A. (2009). Crystal structure of dimeric cardiac L-type calcium channel regulatory domains bridged by Ca^{2+}·calmodulins. Proc. Natl. Acad. Sci. U.S.A. 106: 5135-5140.

Fallon, J. L., Halling, D. B., Hamilton, S. L., & Quiocho, F. A. (2005). Structure of calmodulin bound to the hydrophobic IQ domain of the cardiac Cav1. 2 calcium channel. Structure 13: 1881-1886.

Fan, Y. (2014). The role of AGC3 kinases and calmodulins in plant growth responses to abiotic signals (Doctoral dissertation, Leiden University).

Felle, H. (1988). Auxin causes oscillations of cytosolic free calcium and pH in Zea mays coleoptiles. Planta 174: 495-499.

Friml, J., Yang, X., Michniewicz, M., Weijers, D., Quint, A., Tietz, O., ... & Offringa, R. (2004). A PINOID-dependent binary switch in apical-basal PIN polar targeting directs auxin efflux. Science 306: 862-865.

Galván Ampudia, C. S. (2009). Plant AGC protein kinases orient auxin-mediated differential growth and organogenesis. (Doctoral dissertation, Leiden University).

Galvan-Ampudia, C. S. and R. Offringa. (2007). Plant evolution: AGC kinases tell the auxin tale. Trends Plant Sci. 12: 541-547.

Gehring, C. A., Irving, H. R., & Parish, R. W. (1990). Effects of auxin and abscisic acid on cytosolic calcium and pH in plant cells. Proc. Natl. Acad. Sci. U.S.A. 87(24), 9645-9649.

Gellman, S. H. (1991). On the role of methionine residues in the sequence-independent recognition of nonpolar protein surfaces. Biochemistry 30: 6633-6636.

Gillette, W. K., Esposito, D., Abreu Blanco, M., Alexander, P., Bindu, L., Bittner, C., ... & Stephen, A. G. (2015). Farnesylated and methylated KRAS4b: high yield production of protein suitable for biophysical studies of prenylated protein-lipid interactions. Sci. Rep. 5: 1-13.

Glanc, M., Van Gelderen, K., Hoermayer, L., Tan, S., Naramoto, S., Zhang, X., ... & Friml, J. (2021). AGC kinases and MAB4/MEL proteins maintain PIN polarity by limiting lateral diffusion in plant cells. Curr. Biol. 31: 1918-1930.

Gleave, A. P. (1992). A versatile binary vector system with a T-DNA organisational structure conducive to efficient integration of cloned DNA into the plant genome. Plant Mol. Biol. 20: 1203-1207.

Grant, B. M., Enomoto, M., Back, S. I., Lee, K. Y., Gebregiworgis, T., Ishiyama, N., ... & Marshall, C. B. (2020). Calmodulin disrupts plasma membrane localization of farnesylated KRAS4b by sequestering its lipid moiety. Sci. Signal. 13: eaaz0344.

Harada, A., & Shimazaki, K. I. (2007). Phototropins and blue light-dependent calcium signaling in higher plants. J. Photochem. Photobiol. 83:102-111.

Harada, A., Sakai, T., & Okada, K. (2003). Phot1 and phot2 mediate blue light-induced transient increases in cytosolic Ca^{2+} differently in Arabidopsis leaves. Proc. Natl. Acad. Sci. U.S.A. 100: 8583-8588.

Hasenstein, K. H., & Evans, M. L. (1986). Calcium dependence of rapid auxin action in maize roots. Plant Physiol. 81: 439-443.

Heiman, R. G., Atkinson, R. C., Andruss, B. F., Bolduc, C., Kovalick, G. E., & Beckingham, K. (1996). Spontaneous avoidance behavior in Drosophila null for calmodulin expression. Proc. Natl. Acad. Sci. U.S.A. 93: 2420–2425.

Heissler, S. M., & Sellers, J. R. (2014). Myosin light chains: Teaching old dogs new tricks. Bioarchitecture 4: 169-188.

Heo, W. D., Inoue, T., Park, W. S., Kim, M. L., Park, B. O., Wandless, T. J., & Meyer, T. (2006). PI (3, 4, 5) P3 and PI (4, 5) P2 lipids target proteins with polybasic clusters to the plasma membrane. Science 314: 1458-1461.

Houdusse, A., & Cohen, C. (1995). Target sequence recognition by the calmodulin superfamily: implications from light chain binding to the regulatory domain of scallop myosin. Proc. Natl. Acad. Sci. U.S.A. 92: 10644-10647.

Huang, F., Kemel Zago, M., Abas, L., van Marion, A., Galván-Ampudia, C. S., & Offringa, R. (2010). Phosphorylation of conserved PIN motifs directs Arabidopsis PIN1 polarity and auxin transport. Plant Cell 22: 1129-1142.

Ikura, M., & Ames, J. B. (2006). Genetic polymorphism and protein conformational plasticity in the calmodulin superfamily: two ways to promote multifunctionality. Proc. Natl. Acad. Sci. U.S.A. 103: 1159-1164.

Irving, H. R., Gehring, C. A., & Parish, R. W. (1992). Changes in cytosolic pH and calcium of guard cells precede stomatal movements. Proc. Natl. Acad. Sci. U.S.A. 89: 1790-1794.

Komolov, K. E., Sulon, S. M., Bhardwaj, A., van Keulen, S. C., Duc, N. M., Laurinavichyute, D. K., ... & Benovic, J. L. (2021). Structure of a GRK5-calmodulin complex reveals molecular mechanism of GRK activation and substrate targeting. Mol. Cell 81: 323-339.

Kretsinger, R. H., Rudnick, S. E., & Weissman, L. J. (1986). Crystal structure of calmodulin. J. Inorg. Biochem. 28: 289-302.

Krupnick, J. G., & Benovic, J. L. (1998). The role of receptor kinases and arrestins in G protein-coupled receptor regulation. Annu. Rev. Pharmacol. Toxicol. 38: 289–319.

Landrein, B., Kiss, A., Sassi, M., Chauvet, A., Das, P., Cortizo, M., ... & Hamant, O. (2015). Mechanical stress contributes to the expression of the STM homeobox gene in Arabidopsis shoot meristems. Elife 4: e07811.

Lazo, G. R., Stein, P. A., & Ludwig, R. A. (1991). A DNA transformation–competent Arabidopsis genomic library in Agrobacterium. Biotechnology 9: 963-967.

Lee, J. S., Mulkey, T. J., & Evans, M. L. (1984). Inhibition of polar calcium movement and gravitropism in roots treated with auxin-transport inhibitors. Planta 160: 536-543.

Lefèvre, F., Rémy, M. H., & Masson, J. M. (1997). Alanine-stretch scanning mutagenesis: a simple and efficient method to probe protein structure and function. Nucleic Acids Res. 25: 447-448.

Lu, K. P., Rasmussen, C. D., May, G. S., & Means, A. R. (1992). Cooperative regulation of cell proliferation by calcium and calmodulin in Aspergillus nidulans. Mol Endocrinol. 6: 365-374.

McCormack, E., & Braam, J. (2003). Calmodulins and related potential calcium sensors of Arabidopsis. New Phytol. 159: 585-598.

McLaughlin, S., & Murray, D. (2005). Plasma membrane phosphoinositide organization by protein electrostatics. Nature 438: 605-611.

Michniewicz, M., Zago, M. K., Abas, L., Weijers, D., Schweighofer, A., Meskiene, I., ... & Friml, J. (2007). Antagonistic regulation of PIN phosphorylation by PP2A and PINOID directs auxin flux. Cell 130: 1044-1056.

Monshausen, G. B., Miller, N. D., Murphy, A. S., & Gilroy, S. (2011). Dynamics of auxin-dependent Ca^{2+} and pH signaling in root growth revealed by integrating high-resolution imaging with automated computer vision-based analysis. Plant J. 65: 309-318.

Mori, M. X., Vander Kooi, C. W., Leahy, D. J., & Yue, D. T. (2008). Crystal structure of the CaV2 IQ domain in complex with Ca^{2+}/calmodulin: high-resolution mechanistic implications for channel regulation by Ca^{2+}. Structure 16: 607-620.

Mortuza, S. M., Zheng, W., Zhang, C., Li, Y., Pearce, R., & Zhang, Y. (2021). Improving fragment-based ab initio protein structure assembly using low-accuracy contact-map predictions. Nat. Commun. 12: 5011.

O'Neil, K. T., & DeGrado, W. F. (1990). How calmodulin binds its targets: sequence independent recognition of amphiphilic α-helices. Trends Biochem. Sci. 15: 59-64.

Perochon, A., Aldon, D., Galaud, J. P., & Ranty, B. (2011). Calmodulin and calmodulin-like proteins in plant calcium signaling. Biochimie 93: 2048-2053.

Persechini, A., & Kretsinger, R. H. (1988). Toward a model of the calmodulin-myosin light-chain kinase complex: implications for calmodulin function. J. Cardiovasc. Pharmacol. 12: 1-12.

Plieth, C., & Trewavas, A. J. (2002). Reorientation of seedlings in the earth's gravitational field induces cytosolic calcium transients. Plant Physiol. 129: 786-796.

Poovaiah, B. W., Du, L., Wang, H., & Yang, T. (2013). Recent advances in calcium/calmodulin-mediated signaling with an emphasis on plant-microbe interactions. Plant Physiol. 163: 531-542.

Ranty, B., Aldon, D., & Galaud, J. P. (2006). Plant calmodulins and calmodulin-related proteins: multifaceted relays to decode calcium signals. Plant Signal. Behav. 1: 96-104.

Rhoads, A. R., & Friedberg, F. (1997). Sequence motifs for calmodulin recognition. FASEB J. 11: 331-340.

Sack, J. S., Greenhough, T. J., Bugg, C. E., Means, A. R., & Cook, W. J. (1985). Three-dimensional structure of calmodulin. Nature 315: 37-40.

Sarhan, M., Van Petegem, F., & Ahern, C. A. (2012). Crystallographic basis for calcium regulation of sodium channels. Biophys. J. 102: 325a.

Shen, Y., Maupetit, J., Derreumaux, P., & Tufféry, P. (2014). Improved PEP-FOLD approach for peptide and miniprotein structure prediction. J. Chem. Theory Comput. 10: 4745-4758.

Shih, H. W., DePew, C. L., Miller, N. D., & Monshausen, G. B. (2015). The cyclic nucleotide-gated channel CNGC14 regulates root gravitropism in Arabidopsis thaliana. Curr. Biol. 25: 3119-3125.

Shishova, M., & Lindberg, S. (1999). Auxin-induced cytosol acidification in wheat leaf protoplasts depends on external concentration of Ca^{2+}. Journal of Plant Physiol. 155: 190-196. **Simon, M. L., Platre, M. P., Marquès-Bueno, M. M., Armengot, L., Stanislas, T., Bayle, V., Caillaud, M. C., & Jaillais, Y.** (2016). A PtdIns(4)P-driven electrostatic field controls cell membrane identity and signalling in plants. Nat. Plants 2: 16089.

Takeda, T., & Yamamoto, M. (1987). Analysis and in vivo disruption of the gene coding for calmodulin in Schizosaccharomyces pombe. Proc. Natl. Acad. Sci. U.S.A. 84: 3580–3584.

Thevenet, P., Shen, Y., Maupetit, J., Guyon, F., Derreumaux, P., & Tuffery, P. (2012). PEP-FOLD: an updated de novo structure prediction server for both linear and disulfide bonded cyclic peptides. Nucleic Acids Res. 40: W288-W293

Tidow, H., & Nissen, P. (2013). Structural diversity of calmodulin binding to its target sites. FEBS J. 280: 5551-5565.

Tidow, H., Poulsen, L. R., Andreeva, A., Knudsen, M., Hein, K. L., Wiuf, C., ... & Nissen, P. (2012). A bimodular mechanism of calcium control in eukaryotes. Nature 491: 468-472.

Toyota, M., Furuichi, T., Tatsumi, H., & Sokabe, M. (2008). Critical consideration on the relationship between auxin transport and calcium transients in gravity perception of Arabidopsis seedlings. Plant Signal. Behav. 3: 521-524.

Wang, C., Chung, B. C., Yan, H., Lee, S. Y., & Pitt, G. S. (2012). Crystal structure of the ternary complex of a NaV C-terminal domain, a fibroblast growth factor homologous factor, and calmodulin. Structure 20: 1167-1176.

Wang, P., Shen, L., Guo, J., Jing, W., Qu, Y., Li, W., ... & Zhang, W. (2019). Phosphatidic acid directly regulates PINOID-dependent phosphorylation and activation of the PIN-FORMED2 auxin efflux transporter in response to salt stress. Plant Cell 31: 250-271.

Xu, B., Chelikani, P., & Bhullar, R. P. (2012). Characterization and functional analysis of the calmodulin-binding domain of Rac1 GTPase. PloS one 7: e42975.

Xu, D., & Zhang, Y. (2012). Ab initio protein structure assembly using continuous structure fragments and optimized knowledge-based force field. Proteins. 80: 1715-1735.

Yamniuk, A. P., & Vogel, H. J. (2004). Calmodulin's flexibility allows for promiscuity in its interactions with target proteins and peptides. Mol. Biotechnol. 27: 33-57.

Yang, C. F., & Tsai, W. C. (2021). Calmodulin: The switch button of calcium signaling. Tzu Chi Med. J. 34: 15-22.

Zegzouti, H., Li, W., Lorenz, T. C., Xie, M., Payne, C. T., Smith, K., ... & Christensen, S. K. (2006). Structural and functional insights into the regulation of Arabidopsis AGC VIIIa kinases. J. Biol. Chem. 281: 35520-35530.

Zhang, M., & Vogel, H. J. (1994). Two-dimensional NMR studies of selenomethionyl calmodulin. J. Mol. Biol. 239: 545-554.

Zhang, M., Li, M., Wang, J. H., & Vogel, H. J. (1994). The effect of Met–> Leu mutations on calmodulin's ability to activate cyclic nucleotide phosphodiesterase. J. Biol. Chem. 269: 15546-15552.

Zhang, M., Tanaka, T., & Ikura, M. (1995). Calcium-induced conformational transition revealed by the solution structure of apo calmodulin. Nat. Struct. Mol. Biol. 2: 758-767.

Zhao, X., Wang, Y.L., Qiao, X.R., Wang, J., Wang, L.D., Xu, C.S., & Zhang, X. (2013). Phototropins function in high-intensity blue light-induced hypocotyl phototropism in Arabidopsis by altering cytosolic calcium. Plant Physiol 162: 1539-1551.

Zhukovsky, M. A., Filograna, A., Luini, A., Corda, D., & Valente, C. (2019). Protein amphipathic helix insertion: A mechanism to induce membrane fission. Front. Cell Dev. Biol. 7: 291.

Zourelidou, M., Absmanner, B., Weller, B., Barbosa, I. C., Willige, B. C., Fastner, A., ... & Schwechheimer, C. (2014). Auxin efflux by PIN-FORMED proteins is activated by two different protein kinases, D6 PROTEIN KINASE and PINOID. Elife 3: e02860.

PINOID plasma membrane association and CALMODULIN-LIKE 12/TOUCH 3 binding converge on an amphipathic alpha-helix in the kinase insertion domain